Vortex matter freezing in $Bi_2Sr_2CaCu_2O_8$ samples with a very dense distribution of columnar defects

N. R. Cejas Bolecek,[1] A. B. Kolton,[2] M. Konczykowski,[3] H. Pastoriza,[1] D. Domínguez,[2] and Y. Fasano[1]
[1]*Low Temperature Lab, Centro Atómico Bariloche & Instituto Balseiro, Bariloche, Argentina*
[2]*Solid State Theory Group, Centro Atómico Bariloche & Instituto Balseiro, Bariloche, Argentina*
[3]*Laboratoire des Solides Irradiés, CNRS UMR 7642 & CEA-DSM-IRAMIS, Ecole Polytechnique, Palaiseau, France*
(Received 22 June 2015; revised manuscript received 22 December 2015; published 3 February 2016)

We show that the dynamical freezing of vortex structures nucleated at diluted densities in $Bi_2Sr_2CaCu_2O_8$ samples with a dense distribution of columnar defects, $B \sim 10^{-2} B_\Phi$ with $B_\Phi = 5$ kG, results in configurations with liquidlike correlations. We propose a freezing model considering a relaxation dynamics dominated by double-kink excitations driven by the local stresses obtained directly from experimental images. With this model we estimate the relaxation barrier and the freezing temperature. We argue that the low-field frozen vortex structures nucleated in a dense distribution of columnar defects thus correspond to an out-of-equilibrium nonentangled liquid with strongly reduced mobility rather than to a snapshot of a metastable state with divergent activation barriers as, for instance, expected for the Bose-glass phase at equilibrium.

DOI: 10.1103/PhysRevB.93.054505

I. INTRODUCTION

Vortices nucleated in high-temperature superconducting samples [1] are paradigmatic systems to study the phases frozen in substrates with strong disorder since the relevant energies are easily tuned by changing temperature and magnetic field. Direct imaging techniques [2,3] allow a quantitative analysis of the impact of disorder on the otherwise perfect equilibrium Abrikosov lattice. Magnetic decoration studies [4,5] of quenched vortex structures unveiling a large number of vortices have become a promising avenue to perform these studies [6–10]. This technique provides a two-dimensional top view at the sample surface of the three-dimensional (3D) vortex lattice frozen at $T_{\rm freez}$. In order to move forward on the quantification of the impact of disorder introduced by defects in the vortex structure, better understanding or modeling of the vortex dynamics during the cooling process is necessary. In this work we address this issue by using vortex-defect interaction force magnitudes obtained from magnetic decoration results as input to a theoretical freezing model considering strongly localized vortices.

In field-cooling magnetic decorations, a high-temperature vortex state is driven into a frozen configuration at $T_{\rm freez}$, an intermediate temperature between the initial state and the lower temperatures at which experiments are performed [4,5]. Having a general quantitative understanding of this freezing process is difficult due to the nonequilibrium and nonstationary nature of the three-dimensional thermally activated vortex dynamics over pinning barriers. In order to undergo this study it is then desirable to find a convenient experimental situation in which the vortex dynamics modeling could be simplified. Therefore we have chosen to study the case of a dense distribution of strong pinning centers such as columnar defects (CDs), known to prevail over any other type of crystalline disorder [11–13]. Vortices are then expected to become individually localized at CDs where their thermally activated motion can be modeled in terms of simple excitations, which drive the system into the putative equilibrium Bose-glass phase [14]. Although experimental evidence for the Bose-glass dynamics was reported, the equilibration time and whether the frozen structures observed by magnetic decoration can reveal aspects of this phase for a dense distribution of CDs remain as important open questions.

In this work we study via magnetic decoration the structural properties of vortex matter nucleated in $Bi_2Sr_2CaCu_2O_8$ samples with a large ratio of CDs to vortices, $n_{\rm CD}/n_{\rm v} = B_\Phi/B$, with $B_\Phi = n_{\rm CD}\Phi_0 = 5$ kG the matching field. Although transport and magnetic relaxation experiments were performed for the same system [15–17], the structural properties were previously studied only for smaller doses of CD. A complete destruction of the positional and orientational order of the vortex structure is reported [18–25]. However, for very low CD densities of tens of Gauss, the short-range order of the vortex structure is recovered [19] and a polycrystalline structure is observed in magnetic decoration snapshots [20–25] indicating intervortex repulsion remains important even in the presence of such strong pins. As mentioned, the vortex configurations imaged by field-cooling decorations correspond to the state frozen at $T_{\rm freez}$ at which vortex mobility is strongly reduced by the effect of pinning [2,26]. Here we show that the quenched structures can be well described with a freezing model that considers that the relaxation dynamics of vortices in a dense CD potential is mainly dominated by double-kink excitations. We estimate the value of the relaxation energy barriers from data of the maximum vortex-defect interaction force obtained from magnetic decoration experiments. This allows us to argue that the imaged vortex structures correspond to an experimental time resolution limited frozen nonentangled liquid rather than to a snapshot of the Bose-glass phase characterized by metastable states separated by divergent barriers.

II. EXPERIMENT

The single crystal of optimally doped $Bi_2Sr_2CaCu_2O_8$ studied here was grown by the traveling-floating-zone method [27] and irradiated by 6 GeV Pb ions at GANIL. The irradiation dose was chosen in order to obtain a density of 2.42×10^{10} CDs per square centimeter corresponding to a matching field of $B_\Phi = 5$ kG. Every single ion impact creates an amorphous columnar track with a radius $r_{\rm r} \sim 3.5$ nm, roughly parallel to the c axis through the entire sample thickness.

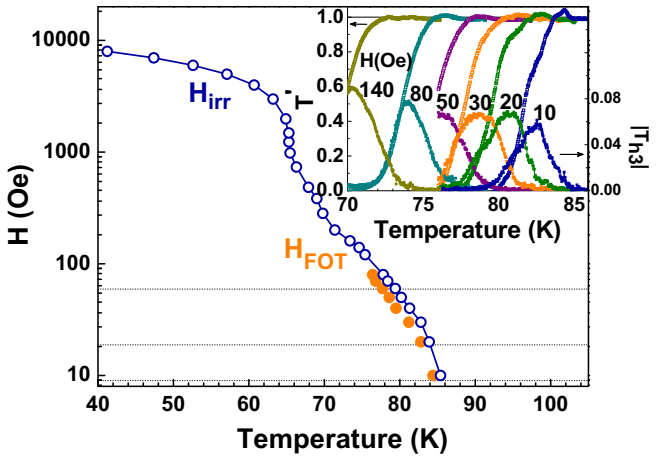

FIG. 1. Vortex phase diagram for $Bi_2Sr_2CaCu_2O_8$ with a dense distribution of CD ($B_\Phi = 5$ kG). Irreversibility, H_{irr}, and first-order, H_{FOT}, transition lines obtained from transmittivity, T', and modulus of the third-harmonic response, $|T_{h3}|$, as explained in the text. Dotted lines indicate the field-cooling processes followed during magnetic decorations. Insert: Temperature dependence of T' and $|T_{h3}|$.

This gives a bare-pinning energy per unit length per CD at zero temperature of $U_0 = \varepsilon_0 \ln[r_r/\sqrt{2}\xi(0)] \sim 6\varepsilon_0(0) \sim 4 \times 10^{-6}$ erg/cm.

The studied crystal was characterized by means of differential magneto-optics [6,28], local Hall-probe magnetometry [29], and magnetic decoration [30] techniques. The sample has a critical temperature $T_c = 86.7$ K, in-plane dimensions of $400 \times 200\ \mu m^2$, and thickness of some tens of μ. Magneto-optical imaging shows rather homogeneous flux penetration into the crystals and does not reveal any noticeable large-scale surface or bulk defect.

The H-T phase diagram of $Bi_2Sr_2CaCu_2O_8$ vortex matter with such a dense distribution of CD was obtained by means of local Hall-probe magnetometry up to 10^5 G, see Fig. 1. These measurements were done using microfabricated 2D-electron-gas Hall magnetometers that locally probe the sample stray field [29]. Magnetic transmittivity measurements were performed by applying an ac excitation field H_{ac} parallel to a dc field H. The Hall data presented here were obtained with an excitation field of 1.2 Oe rms and 11 Hz. A digital-signal-processing lock-in technique is used to simultaneously measure the in- and out-of-phase components of the fundamental and the third-harmonic signals of the Hall voltage. The fundamental signal was used to obtain the thermodynamic first-order transition line [31,32], $H_{FOT}(T)$, from transmittivity T' measurements [33]. The third-harmonic signal $|T_{h3}|$ yields information on the onset of irreversible magnetic behavior at $H_{irr}(T)$ [33].

The structural properties of vortex matter nucleated on the same crystal were directly imaged by means of magnetic decoration experiments [30]. This study was limited to magnetic fields below 80 Oe since for this sample the technique looses single-vortex resolution at larger vortex densities. The sample was field cooled from $T > T_c$ down to 4.2 K in roughly 15 min and magnetic decorations were performed at this base temperature. The structural properties, at the length scales of the lattice parameter, correspond to those frozen at T_{freez}. By using quantitative information obtained from magnetic decoration images we will estimate T_{freez} according to the freezing dynamics model presented in Sec. IV.

III. EXPERIMENTAL RESULTS

A. Vortex phase diagram

Figure 1 shows the vortex phase diagram of $Bi_2Sr_2CaCu_2O_8$ vortex matter nucleated in samples with a CD density of $B_\Phi = 5$ kG. The first-order, H_{FOT}, and irreversibility, H_{irr}, lines are obtained from measuring the sample magnetic response by means of ac Hall magnetometry [33]. The insert shows the temperature evolution of normalized first- and third-harmonic signals in the low-field range. The transmittivity T' is obtained from the in-phase component of the first-harmonic signal [34], and is highly sensitive to discontinuities in the local induction, as for example the one entailed at the H_{FOT} transition [31,32]. The normalized modulus of the third-harmonic signal, $|T_{h3}|$ [34], becomes non-negligible at the onset of nonlinear response arising from irreversible magnetic properties.

The high-temperature H_{FOT} transition is detected in ac transmittivity measurements as a frequency-independent so-called paramagnetic peak that develops in T' at the same H as the jump in local induction detected in dc hysteresis loops [33,35]. The paramagnetic peak is equivalently observed in T' versus temperature curves, see Fig. 1. For the studied sample the paramagnetic peak is clearly observed in T' curves up to 80 Oe. The irreversibility line is identified from the frequency-dependent onset of $|T_{h3}|$ on cooling [36]. In the range $H < B_\Phi/6$, T_{irr} monotonically shifts towards lower temperatures on increasing field, whereas for $B_\Phi/6 < H < B_\Phi/3$ becomes almost field independent. At larger fields, a monotonous increase of H_{irr} with reducing field is again observed. This field evolution of the irreversibility line is common to $Bi_2Sr_2CaCu_2O_8$ samples with high densities of CD and has origin in the three different regimes for the occupation of columnar defects with vortices discussed in Refs. [37,38].

Figure 1 also indicate with dotted lines the H-T paths followed during the field-cooling magnetic decoration experiments. For all the imaged vortex structures the system undergoes the melting transition at $T_{FOT} \sim 0.98 T_{irr}$. This shifting between both lines, although of lesser intensity, was also reported in pristine samples [36].

B. Structural properties of the frozen vortex matter

Figure 2 shows snapshots of the vortex structure obtained in field-cooling magnetic decoration experiments at applied fields of 10, 20, and 60 Oe. Due to the finite magnetization of these samples with pinning enhanced by CD, the local induction measured from the vortex density is smaller than the applied field, $B = 9$, 18.8, and 59.4 G, respectively. In this field range vortices are extremely diluted with respect to the random distribution of CD, every vortex unit cell spanning a spatial region having between 80 (60 Oe) and 500 (10 Oe) defects. In this limit, one can expect that the vortex structure presents similar topological order than in the case of pristine samples. Strikingly, the observed vortex structures are amorphous,

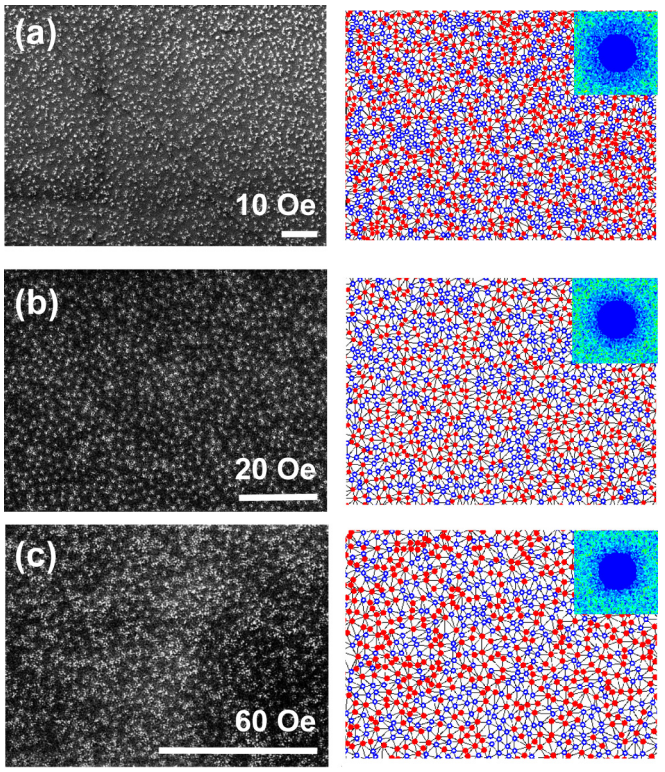

FIG. 2. Vortex structure in $Bi_2Sr_2CaCu_2O_8$ samples with a CD density corresponding to $B_\Phi = 5$ kG for applied fields of (a) 10, (b) 20, and (c) 60 Oe. Left panels: Magnetic decoration images of the vortex structure taken at 4.2 K after field cooling from the liquid vortex phase. The white bars correspond to 10 μm. Right panels: Delaunay triangulations indicating first-neighbors and sixfold (blue) and nonsixfold (red) coordinated vortices. The inserts show the Fourier transform of the vortex positions.

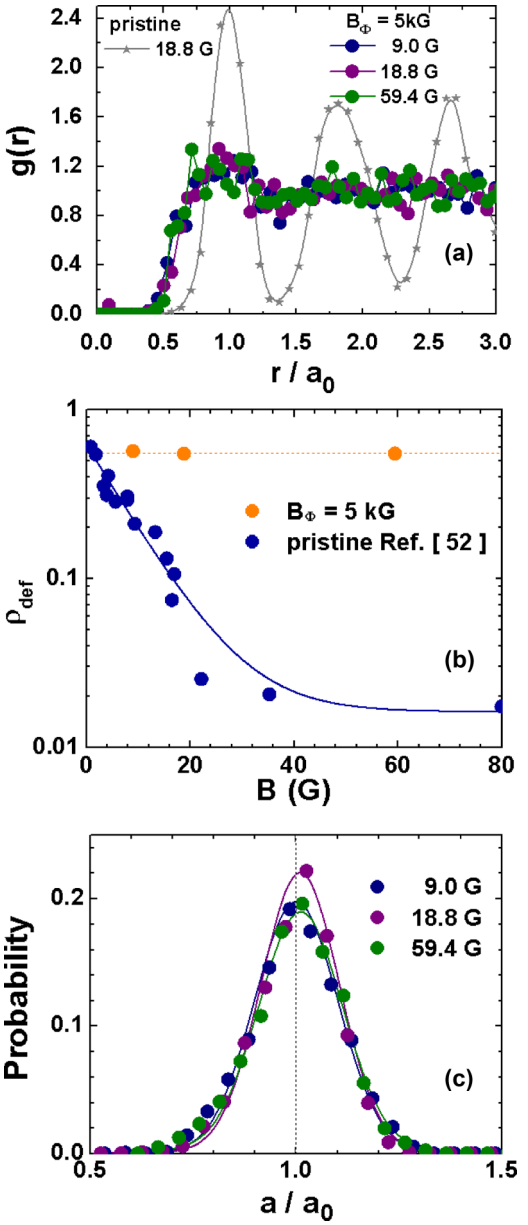

FIG. 3. Structural properties of $Bi_2Sr_2CaCu_2O_8$ vortex matter nucleated in samples with a dense distribution of CD corresponding to $B_\Phi = 5$ kG. (a) Pair-correlation function for the vortex structures nucleated at several fields (circles). For comparison, we show the results in a pristine sample at 18.8 G. (b) Field-evolution of the density of nonsixfold coordinated vortices obtained from the images of Fig. 2 as compared to the case of vortex matter nucleated in pristine samples. Lines are guides to the eye. (c) Distribution of first-neighbors distances, a, normalized by the average lattice spacing a_0 (points). The full lines are fits to the data with Gaussian functions.

irrespective of the vortex density within the studied range. These results follow the same trend as magnetic decoration data on samples with a less-dense distribution of CD ($B_\Phi = 3.5$ kG) where a complete destruction of translational order was reported [18].

The Delaunay triangulations of the right panels of Fig. 2, indicating the first neighbors for each vortex, reveal that the structures have the nonsixfold coordination typical of an amorphous structure. The ringlike patterns of the Fourier transform of vortex positions shown in the insert confirm the lack of short-range positional and orientational orders. Indeed, the pair correlation functions $g(r)$ of Fig. 3(a) show only one distinguishable peak at the first-neighbors distance, irrespective of significantly increasing the intervortex interaction. This contrasts with the $g(r)$ obtained for pristine samples that present peaks up to several lattice spacings [see the curve with stars in Fig. 3(a)]. The sixfold coordinated vortices (blue) form very small crystallites containing at best 10 vortices. The density of these vortices is always below 40% and does not vary significantly on increasing field, see Fig. 3(b). Quantitatively similar results are obtained for samples with a much more diluted distribution of CD when $\sqrt{B/B_\Phi} < 1.1$ [22]. Figure 3(b) also shows that the density of vortices belonging to topological defects, $\rho_{\rm def}$, is significantly larger in samples with a dense distribution of CD than in the case of vortex matter nucleated in pristine $Bi_2Sr_2CaCu_2O_8$ samples [2]. However, since magnetic decoration images are snapshots of the vortex structure, distinguishing between an amorphous glassy and a liquid vortex phase is not possible with this technique.

Similar amorphous structures were recently reported for the strongly pinned vortex matter in pnictide $BaFe_2(As_{1-x}P_x)_2$

and $Ba(Fe_{1-x}Co_x)_2As_2$ samples [6,8], presenting significant vortex-density fluctuations, more pronounced in the Co-doped system. The disorder of the vortex structure was quantitatively ascribed to the strong inhomogeneous disorder present in the samples [6]. On the contrary, in the $Bi_2Sr_2CaCu_2O_8$ samples studied here, vortex density fluctuations are not very strong, as observed in the histograms of a/a_0 shown in Fig. 3(c). These histograms are well fitted by a symmetric Gaussian distribution with full width at half maximum ranging 23–20 %. The data are normalized by the lattice parameter $a_0 = 1.075\sqrt{\Phi_0/B}$, with B obtained from the vortex density measured in magnetic decoration images.

In the field-cooling magnetic decoration experiments performed here, vortex matter is nucleated in the high-temperature liquid phase and vortices have a high mobility since the decoupled pancakes present a low shear viscosity. On cooling, vortex mobility gets reduced at $T_{\rm freez}$ by the effect of the CD pinning potential and the vortex structure gets frozen, at length scales of the lattice parameter a_0, in one of the many available metastable states. On further cooling to lower temperatures, vortices accommodate in order to profit from the pinning potential in all their length at length scales of the order of coherence length, $\xi \ll a_0$, a length scale that can not be resolved by means of magnetic decoration. As a consequence, the structural properties of vortex matter revealed by magnetic decorations at 4.2 K correspond to those of the structure frozen at $T_{\rm freez}$. Therefore this is the temperature that has to be considered in order to evaluate elastic and electromagnetic properties of vortex matter observed by means of magnetic decoration. As usually considered in the literature [2,26], it is reasonable to assume $T_{\rm freez} \sim T_{\rm irr}$ since at this temperature pinning becomes dominant over the other energy scales. However, there can be a shift between these two temperatures: The model presented in Sec. IV will allow us to discuss the validity of this assumption and its implications.

C. Vortex-defect force distributions

In spite of the absence of important fluctuations in vortex density, the pinning potential generated by a dense distribution of CD produces a strong impact in the lattice structural properties, particularly evident in the spatially inhomogeneous intervortex interaction energy and vortex-defect force. We will focus our study on the last magnitude since from its probability distribution we will get the experimental information considered as input to evaluate the typical energy barriers considered in the freezing dynamics model we propose in Sec. IV. The vortex-defect force is related to the intervortex repulsive force, $\mathbf{f}_i$. Figure 4 shows maps of the magnitude of this force per unit length for each vortex i, $f_i \equiv |\mathbf{f}_i|$, computed as the modulus of

$$\mathbf{f}_i = \sum_j \frac{2\varepsilon_0}{\lambda_{ab}} \frac{\mathbf{r}_{ij}}{|\mathbf{r}_{ij}|} K_1\left(\frac{|r_{ij}|}{\lambda_{ab}}\right). \quad (1)$$

K_1 is the first-order modified Bessel function, λ_{ab} the in-plane penetration depth, and $\varepsilon_0 = (\Phi_0/4\pi\lambda_{ab})^2$ the vortex line-tension. The sum is performed up to a cutoff radius $r_{\rm cut} = 10a_0$ since $\mathbf{f}_i$ does not change significantly when including terms at larger distances. For every magnetic field, $\mathbf{f}_i$ is calculated considering the value of the penetration depth at the temperature at which the vortex structure is frozen that we approximate by $T_{\rm irr}$. We have considered the $\lambda_{ab}(T/T_c)$ evolution reported in Ref. [13] for pristine $Bi_2Sr_2CaCu_2O_8$ samples and calculated $\lambda_{ab}(T_{\rm irr}/T_c)$ from the data of the vortex phase diagram shown in Fig. 1; λ_{ab} for samples with a density of CD of $B_\Phi = 5$ kG is within 1% of this value [37].

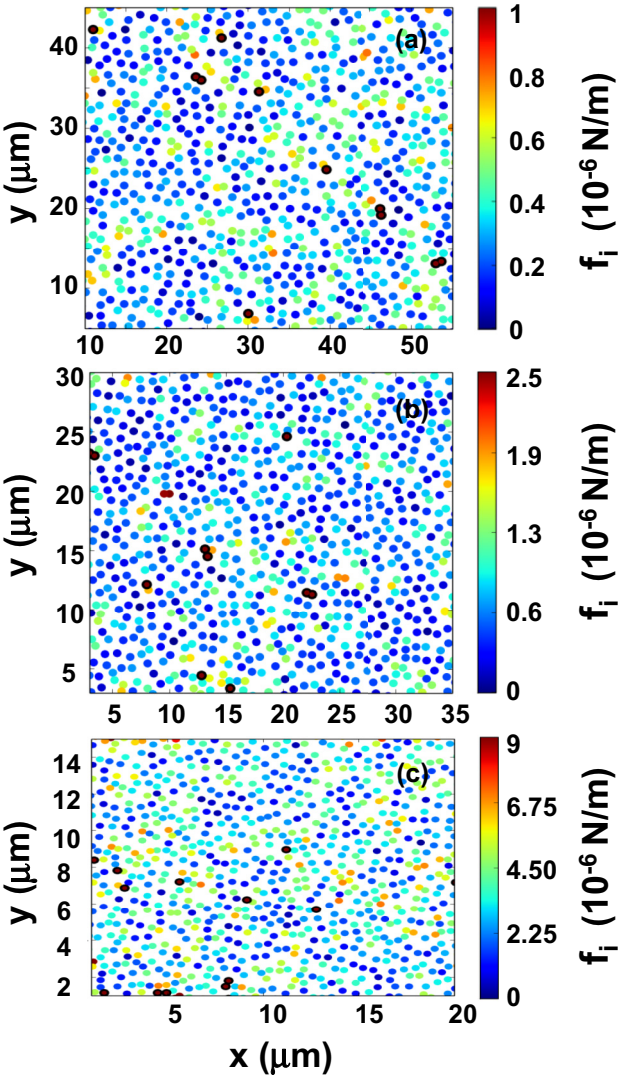

FIG. 4. Color-coded maps for the modulus of the intervortex repulsive force for vortex densities of (a) 9, (b) 18.8, and (c) 59.4 G corresponding to the decoration images of Fig. 2. Vortices with modulus of the intervortex repulsive force larger than the mode value plus half width at half maximum are highlighted in black.

Since the vortex structures frozen during field-cooling processes are close to metastable equilibrium at $T_{\rm freez}(B)$, nonzero values of f_i can only be ascribed to the force exerted by the CD pinning potential to individual vortices. Therefore the f_i maps are an accurate estimation of the minimum vortex-defect force at the local scale. These maps are highly inhomogeneous and present clusters with larger intervortex force magnitude. The f_i histograms of Fig. 5(a) show that the mode value monotonically enhances with increasing vortex density. In addition, the distributions are not symmetric and have a larger weight in the high-force part. On increasing B, the f_i distributions broaden significantly and get more asymmetric.

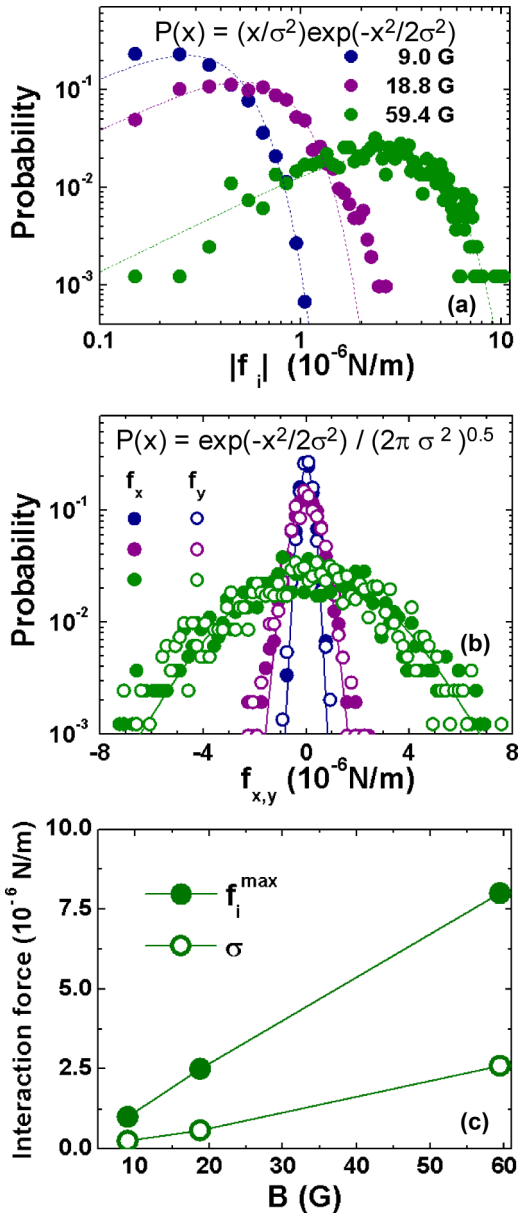

FIG. 5. Distributions of the intervortex repulsive force per unit length for $Bi_2Sr_2CaCu_2O_8$ samples with a dense distribution of CD at different vortex densities. (a) Modulus of the intervortex force (points) and fits to the data with the Rayleigh function indicated (dotted lines). (b) Distributions of the x- (full points) and y- (open points) components of the intervortex force and fits with a symmetric Gaussian distribution (full lines). (c) Standard deviation and maximum values of the intervortex force modulus distributions as a function of vortex density.

Figure 5(b) shows the histograms of the x and y components of the interaction force, f_x and f_y. In contrast to the f_i distributions, the force-components distributions are symmetric with respect to zero and their width increases with field. The f_x and f_y distributions are properly fitted with Gaussian functions (see dotted lines), implying that the individual components of the force varies at random. Therefore, a Rayleigh functionality should be expected for the distribution of the modulus of the force. The fits shown with dotted lines in Fig. 5(a) (see the mathematical expression on the top) indicate that the distributions of $\mathbf{f}_i$ follow reasonably well this functionality. Therefore the increasing asymmetry of the f_i distributions with B comes from the increment of the standard deviation of the Gaussian distributions that follow the components of the force.

Finally, Fig. 5(c) shows that the dispersion obtained from the Rayleigh fits to the f_i distributions, σ, as well as the maximum value of the defect-vortex pinning force, f_i^{max}, increase monotonically with field. Considering that the CD pinning force is finite and has a maximum value of $f_c = U_0/r_r$, extrapolating to higher fields the data shown in Fig. 5(c) yields $f_i^{max} \sim f_c$ at around 4000 G. This suggests a crossover towards vortex configurations with insterstitial vortices, i.e., not located on a CD, at fields $B{\sim}0.8B_\Phi$.

Assuming that localized vortices relax the local excess stress by simple single-vortex excitations, linear extrapolation of f_i^{max} also allows the estimation of the field at which half-loop excitations are exhausted in favor of double-kink excitations [14]. This occurs when $f_i^{max} \sim f_d \approx U_0/d = f_c(d/r_r) \approx f_c/20$. Hence, for $B{\sim}0.04B_\Phi$ we predict the extinction of half loops at very short times. Comparing with the maximum field we analyze, $B = 0.01B_\Phi$, we can argue that relaxation will be dominated by double kinks first and by superkinks only in the long-time limit. This kind of argument, combined with the magnitude $f_i^{max}(B)$ obtained from the vortex structures frozen during field-cooling magnetic decoration experiments allowed us to estimate the typical energy barriers and relaxation times considered in the freezing dynamics model presented in the next section.

IV. FREEZING DYNAMICS MODEL

In this section we discuss the experimental results in terms of a simple model for the dynamics of freezing of the vortex structure during field cooling in the presence of the strong disorder associated to a dense distribution of CD. This model allows us to estimate the lifetime of the observed metastable vortex configurations and T_{freez} from characteristic parameters of the system and considering information obtained from magnetic decoration images taken at low fields and 4.2 K (see Fig. 2). We will assume that columnar disorder is strong and dense ($B \ll B_\Phi$) such that, for temperatures of the order of T_{freez}, well defined vortex lines remain most of the time individually pinned in a single columnar defect. Namely, in this model we neglect the effect of point disorder.

During the freezing process, pinned vortices form metastable configurations α characterized by the set of occupation numbers of each CD, $\alpha \equiv \{n_k\}$, where $n_k = 1$ if the kth CD is occupied by a vortex, and $n_k = 0$ otherwise. In each metastable state the interaction force f_i must balance in average the defect-vortex force on vortex i. During the lifetime of the metastable state, controlled by thermal activation, vortices are bound to their columnar defects, only performing small futile fluctuations. Near freezing, the lifetime of metastable states are expected to be comparable to experimental times, and their typical configurations similar to the ones observed by magnetic decoration. We are thus considering that cooling down to 4.2 K for magnetic decoration has only the effect of further stabilizing the metastable configuration frozen at T_{freez}. We will use this criterion for inferring information about the

dynamics near the freezing of the observed vortex structures and ultimately unveil the relevant excitations that will allow us to discern on the nature of the frozen vortex structure.

In order to model the nonstationary dynamics connecting different metastable states after a temperature quench, we will assume that the relaxation process is mainly dominated by single vortex hopping between the randomly distributed CDs. We are thus neglecting multiple vortex hopping, which might be important at higher vortex densities. For simplicity, we will consider identical CDs, the so-called nondispersive case [1]. Under this assumption, the contribution of superkink excitations is not relevant and thus the optimal thermal excitations of an individual vortex line are either half loops or double kinks (DKs) [1]. These excitations allow a vortex to escape from one columnar defect, and to be then retrapped by a nearby defect located at a typical distance $d \sim (\Phi_0/B_\Phi)^{1/2} \ll a_0$. Since we also have $d \ll \lambda_{ab}(0) < \lambda_{ab}(T)$, the vortex-defect force on vortex i is practically the same for consecutive metastable states. If we denote the metastable state at a given time by a supraindex α, the relaxation process connecting different metastable states can thus be effectively viewed as a nonsteady transport process driven by the heterogeneous set of average local forces associated to the metastable state, $\{\mathbf{f}_i^\alpha\}$. The dependence of f_i with α allow us to include the nonsteady variation of vortex-vortex interactions during the relaxation and its magnetic field dependence.

Half-loops excitations are expected to be relevant for pinned vortices such that $f_d < f_i^\alpha < f_c$, where $f_d \approx U_0/d$ is the force at which a half loop involves a displacement of the order of the average separation between defects, d, and $f_c \approx U_0/r_r$ is the critical depinning force from a single defect. As we show below, half loops drive the relaxation at very short time scales; for larger times most local forces f_i^α drop below f_d and half-loop excitations are exhausted. Figure 6 shows a schematic representation of the relevant excitations at each time scale. Therefore, at large time scales relaxation is mainly driven by DK excitations since most of vortices feel an interaction force $f_i < f_d$ from the other vortices. Optimal DKs have a longitudinal length $z \approx d\sqrt{\epsilon_l/U_0}$ and cost an energy $2E_K \approx 2d\sqrt{\epsilon_l U_0}$. The line tension $\epsilon_l \sim \varepsilon_0/\Gamma^2$ is normalized by the anisotropy of the vortex system Γ, and corresponds to the limit of short-wavelength distortions in the c direction involved in the kink formation. The proliferation of optimal DK excitations allows a vortex localized at a defect to hop to a neighbor one at a distance of the order of d. Provided that the energy barrier for such excitation, $U_i^\alpha = (2E_K - f_i^\alpha dz)$, is larger than $k_B T$, the typical time to escape from the defect is given by the Arrhenius law $\tau_i^\alpha = \tau_0 e^{U_i/k_B T}$, yielding

$$\tau_i^\alpha \approx \tau_0\, e^{(2d\sqrt{\epsilon_l U_0} - d^2\sqrt{\epsilon_l/U_0} f_i^\alpha)/k_B T}, \tag{2}$$

where τ_0 is a characteristic time, or inverse of the attempt frequency. The last formula is an estimate for the escape time of a vortex i feeling the interaction force f_i^α with all the other vortices on a given metastable state α.

We can define the lifetime of a given metastable configuration α as the minimum single-vortex escape time among all vortices, as one vortex hop changes a pair of CD occupation numbers, producing a new metastable state α'. Such a minimal escape time corresponds to the minimal escape barrier $U^\alpha = \min_i[2d\sqrt{\epsilon_l U_0} - d^2\sqrt{\epsilon_l/U_0} f_i^\alpha]$. Therefore, it corresponds to the escape time of the least bounded vortex, feeling the maximum force $f_{max}^\alpha = \max_i[f_i^\alpha]$ in the metastable configuration α. Remembering that $U_0 \sim \varepsilon_0(r_r^2/2\xi^2)$, we finally get the escape time for a given metastable configuration

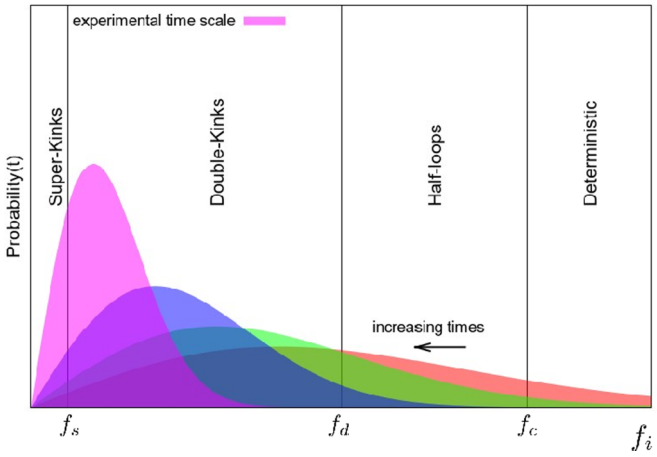

FIG. 6. Schematic picture for the distribution of the local force relaxation process in the limit $d \ll a_0, \lambda_{ab}$. The system starts from a highly disordered state with a broad distribution of local forces. As relaxation goes on, the force distribution becomes narrower and the system gets quickly trapped into metastable states when all forces lie below f_c. Thermally activated optimal hops then allow vortices to escape from their CDs via different mechanisms: half loops for $f_d < f < f_c$, double-kinks for $f_s < f < f_d$, and superkinks for $f < f_s$ (for identical CDs $f_s = 0$), where f_c and f_d depend on the pinning energy, radius and separation between CD and f_s also depends on the degree of CD disorder. During a field-cooling process, the distribution becomes practically frozen at a temperature T_{freez} for the experimental time scale.

$$\tau^\alpha \approx \tau_0 \exp\left[\frac{U^\alpha(a_0,\lambda_{ab},d,r_r)}{k_B T}\right], \tag{3}$$

where we have defined the effective energy barrier associated with a given pinned configuration α,

$$U^\alpha \equiv U^\alpha(a_0,\lambda_{ab},d,r_r) = \left[1 - \frac{\tilde{f}_{max}^\alpha(a_0,\lambda_{ab})d\lambda_{ab}}{2\kappa^2 r_r^2}\right] 2E_K, \tag{4}$$

as a function of the characteristic lengths a_0, λ_{ab}, d, and r_r. The dimensionless force $\tilde{f}_{max}^\alpha = f_{max}^\alpha \lambda_{ab}/2\varepsilon_0$, is defined as

$$\tilde{f}_{max}^\alpha(a_0,\lambda_{ab}) = \max_i \left| \sum_{j\neq i} K_1(\mathbf{r}_{ij}/\lambda_{ab}) \frac{\mathbf{r}_{ij}}{r_{ij}} \right|, \tag{5}$$

obtained from the $\mathbf{f}_i^{max}$ data shown in Fig. 5(c). Therefore α corresponds to the metastable state frozen during the field-cooling decoration experiment. The DK energy cost can be written in terms of the characteristic lengths λ_{ab}, d, and r_r as

$$2E_K \equiv 2E_K(\lambda_{ab},d,r_r,\Gamma,\kappa) = \sqrt{2}\frac{\kappa r_r d\varepsilon_0}{\lambda_{ab}\Gamma}. \tag{6}$$

Within this model, the field dependence of the lifetime comes from the field dependence of the maximum value of the defect-vortex force distribution for the given frozen configuration. The insert to Fig. 7 shows that the lifetime weakly

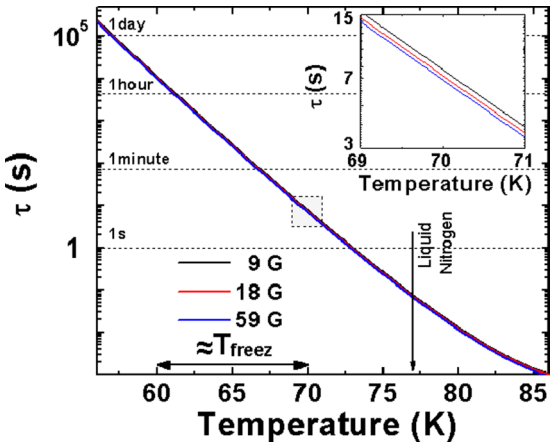

FIG. 7. Lifetime of the decorated metastable vortex configuration vs temperature, assuming only double-kink excitations during the out of equilibrium relaxation. We indicate the estimated freezing temperature T_{freez} at which the vortex structure is frozen at length scales of a_0 as revealed by magnetic decoration. The inset shows a weak decrease of the lifetime with increasing the magnetic field for the field range analyzed.

decreases with increasing the magnetic field. Extrapolation of the behavior of Fig. 5(c) to larger fields suggests that this trend continues, and that T_{freez} should therefore also decrease with increasing magnetic field, following qualitatively the behavior of T_{irr} in Fig. 1.

Let us first estimate the lifetime τ of the decorated metastable vortex configurations—we will drop the supraindex α when referring to the frozen metastable state– - by making again the reasonable assumption that they were frozen at, or very near to, the irreversibility line, namely $T_{freez} \approx T_{irr}$. From expressions of Eqs. (3), (4), (5), and (6), we get the results for the escape time τ shown in Table I, using as input the dimensionless force $\tilde{f}^{\alpha}_{max}$ evaluated from the experimental data and the sample characteristics indicated in the caption of the table. In all cases we verified that $\tilde{f}_d(\lambda_{irr}) > \tilde{f}_{max}(\lambda_{irr})$ so that half-loop excitations are not relevant. The estimated lifetimes of Table I, of the order of $\tau_0 \sim 10^{-3}$ s, are much smaller than the typical time scales of decoration experiments, namely $\tau(T_{irr}) \ll \tau_{exp}$, with τ_{exp} of the order of seconds or minutes. Therefore, we should necessarily have $T_{freez} < T_{irr}$ since the freezing temperature should correspond to $\tau(T_{freez}) \sim \tau_{exp}$. Forcing such a condition, from Eqs. (3), (4), (5), and (6) we can estimate the value of T_{freez}. In order to do this realistically, we need to know the temperature dependence of λ_{ab} at $T < T_{irr}$. Here, we will simply assume the dependence $\lambda_{ab}(T) = \lambda_{ab}(0)/\sqrt{1-(T/T_c)^4}$ with $\lambda_{ab}(0) = 180$nm. This dependence yields a reasonable analytical approximation for the values reported at $T \sim T_{irr}$ [13] and shown in Table I for $T = T_{irr}(B)$ for the B studied here.

Recalculating $\tilde{f}^{\alpha}_{max}$ and U^{α} as a function of T using this approximation for $\lambda_{ab}(T)$, and setting $\tau(T_{freez}) \sim \tau_{exp}$, with τ_{exp} ranging from seconds to hours, we get freezing temperatures in the range $T_{freez} \approx 60$–70 K as shown in Fig. 7. The insert to this figure shows that the field dependence of the lifetime, and thus of $\tau(T_{freez})$, is very weak. Indeed the experimentally detected change in almost one order of magnitude in $\mathbf{f}_i^{max}$ on increasing field only impacts in changing $\sim$5% the escape time at T_{irr}, a magnitude that is even smaller at lower temperatures due to the decrease of $\lambda_{ab}(T)$. It is also interesting to note that at the liquid nitrogen temperature T_N, at which the sample spends some minutes during the magnetic decoration cooling protocol down to 4.2 K, the dynamics is relatively fast, with lifetimes of roughly milliseconds. This means that the frozen configuration has a memory of a temperature $T_{freez} < T_N$, indicated in Fig. 7.

We conclude our theoretical analysis discussing the validity of some of the main assumptions of our model. We have assumed that CDs are perfectly parallel to the applied magnetic field, so vortices individually localize in a single defect before a thermally activated event drives it to a neighbor, a more favorable pin. However, in the experiments there might exist a misalignment between the applied field and the CD direction of less than five degrees. At low temperatures, below the irreversibility line, pinned vortices aligned with a single CD are stable only below the characteristic tilting locking angle θ_L, between the applied field and the defects. For misalignments larger than θ_L vortices can still feel the effect of CD but develop a kinked structure (staircaselike) connecting more than one defect. Only above a larger characteristic trapping angle θ_t, vortices are not locked by CD and the response to a tilt becomes linear [14]. For $Bi_2Sr_2CaCu_2O_8$ irradiated with a $B_\Phi = 5$ kG dose, for $T \sim T_{irr}$ and $B \ll B_\Phi$, our experimental conditions, a trapping angle $\theta_t \approx 60$–75 degrees was experimentally determined in Refs. [15,40]. Being CD efficient to pin and deform the vortices even for such large angles, their effect for misalignments one order of magnitude smaller should be much stronger. To our knowledge the locking angle θ_L (below which perfect alignment is expected as it is assumed in our model), has not been experimentally determined for the irradiation dose of our sample. However, it can be theoretically estimated as $\theta_L = (4\pi\epsilon_l/\Phi_0 H)\theta_t$ [1]. Using the reported experimental value $\theta_t \approx 60$–75 degrees, and the line tension ϵ_l corresponding to our material, we get $\theta_L \approx 3$–15 degrees for the three fields we have studied. It is worth noting that these values are in accordance with the experimental value $\theta_L \approx 20$ degrees measured for $YBa_2Cu_3O_7$ with the same dose, at fields and temperature similar to ours [41], if we take into account explicitly the anisotropy ratio of both systems. Since $\theta_L \sim 3$–15 degrees is of the order or larger than our experimental uncertainty of five degrees, we conclude that the

TABLE I. Estimation of the lifetime τ of the magnetically decorated metastable vortex configurations frozen during field cooling at $\sim T_{irr}$ and assuming only DK excitations. We have used the following sample characteristics: $d = 0.065 \times 10^{-4}$cm, $r_r = 3.5 \times 10^{-7}$cm, $(d/r_r \sim 20)$, $\lambda(T=0) = 0.18 \times 10^{-4}$cm, $T_c = 86.7$ K, $\kappa \approx 200, \Gamma \approx 150$. The parameters $\lambda_{irr} = \lambda(T_{irr})$ and $\epsilon_0^{irr} = (\Phi_0/4\pi\lambda_{irr})^2$. The characteristic value $\tau_0 \sim 10^{-3}s$ is taken from the frequency-dependent ac creep measured in samples from the same batch than ours [15].

B [G]	$\lambda_{ab}(T_{irr})$ [μm]	T_{irr} [K]	$\tilde{f}_{max}$ [$\lambda_{ab}(T_{irr})$]	U/k_B [K]	τ [s]
9	0.69	85.3	0.6	26	0.0013
18.8	0.59	83.9	0.97	41	0.0016
59.4	0.39	79.6	0.87	142	0.0059

perfect alignment assumption of our model is fairly acceptable. Indeed, even for tilting angles $\theta \gtrsim \theta_L$ the typical distance between these kinks is expected to diverge as $(\theta - \theta_L)^{-1/2}$ as we approach θ_L [14]. Therefore, perfect alignment is then possible even for $\theta \gtrsim \theta_L$ due to a finite size effect, when the distance between kinks become of the order of the sample width, in our case $\sim 50\ \mu$m.

In our model we have neglected the contribution of half-loop excitations. As argued in the previous section this is justified from the fact that these excitations are important for forces smaller than $\tilde{f}_c = (U_0/r_r)(\lambda_{ab}/2\epsilon_0) \approx 100$ and larger than $\tilde{f}_d = \tilde{f}_c(r_r/d) \approx \tilde{f}_c/20 \approx 5$ at T_{irr}, which is larger than the adimensional forces of Table I for the range of magnetic fields analyzed. Half loops would thus drive the relaxation only at very short times after the quench. We have also neglected the dispersion in the CD pinning energy. This dispersion is produced both by the on-site dispersion, (typically arising from the unavoidable dispersion in the ions tracks diameters), or by the intersite dispersion (arising from the dispersion in the nearest-neighbor distance between tracks, which is indeed expected to be Poisson distributed). According to Ref. [17], the main source of energy dispersion comes from the diameter dispersion, which for 5.8 GeV Pb ions was estimated to be of the order of 15%. This implies an energy dispersion $\Delta U_0/U_0 \sim 2.5\%$ at zero temperature. The crossover force f_s from double-kink to superkink excitations is thus of the order of $f_s \approx f_d(\gamma/U_0) \approx f_d(\Delta U_0/U_0) = f_d/40$. Since for our case $f_d = U_0/d \approx 202\epsilon_0/\lambda$, we get the adimensional force $\tilde{f}_s \equiv f_s(\lambda_{ab}/2\epsilon_0) \sim 0.5$. From these estimates we first note that the characteristic force extracted from magnetic decoration images is $\tilde{f}_{max} \sim 1$ (see Table I). Since $\tilde{f}_s \sim \tilde{f}$, the typical hopping distance in the variable range hopping on netoregime [1] becomes $u_{VRH} \approx d(f_v/f)^{1/3} \sim d$. We thus conclude that the dominance of DK excitations between columnar tracks separated by a typical distance d in the direction of the local force is a fair approximation for the most common elementary excitations driving the relaxation near T_{freez}.

Finally, we have also neglected the possible thermal renormalization of the pinning potential expected to become important above a characteristic temperature [14] $T_1 \approx T_c(r_r/4\xi)\sqrt{\ln\kappa/Gi}/[1 + (r_r/4\xi)\sqrt{\ln\kappa/Gi}]$. Using parameters for $Bi_2Sr_2CaCu_2O_8$, $Gi = 10^{-2}$, $\kappa = 200$, $r_r = 35$nm, and $\xi = 1$nm we get $T_1 \approx 72$ K, which is of the order of the T_{irr} for the range of magnetic fields analyzed but larger than our estimated T_{freez}. Therefore, thermal renormalization of the pinning energies is expected to be weak, justifying our approximation.

V. DISCUSSION

The predictions from the model discussed in the previous section, based on quantitative information obtained from decoration experiments at 4.2 K, suggest that the decorated structures were dynamically frozen at a much larger temperature T_{freez} by the strong decrease of vortex mobility with temperature induced by the CD dense pinning potential. Within the model, this mobility is dominated by Arrhenius activation through the temperature-dependent finite barriers associated with DK excitations, as barriers for half loops can be overcome in typical times of the order of milliseconds while the larger barriers expected for superkinks were disregarded on the basis that DK alone are able to yield metastable states with macroscopic lifetimes. Within this scenario, it is worth mentioning that previous works studying samples with $B_\Phi = 5$ kG from the same batch as ours reported that the low-field regime presented nondivergent activation barriers varying linearly with the ac driving current [15]. This is in contrast to the divergent barriers found at higher fields, consistent with half-loop excitations. On the other hand, it was proposed that for a high density of CD the change in pinning energies when increasing field are negligible compared to the change in interaction energy, giving place to a discrete superconductor picture [38]. These two findings are consistent with our model assumption that the relevant excitations driving the nonsteady relaxation are just DK, and that the role of superkink excitations is not important for the time scales typical of our magnetic decoration experiments.

Note that this is in contrast with the barriers expected, for instance, for the Bose glass phase, which tend to diverge near equilibrium, a signature of the strong localization of vortex lines at very long times with a broad variable range hopping. The amorphous order observed in the decorations can then be interpreted as a snapshot of a nonentangled liquidlike structure metastable at T_{freez}, a temperature located below the first-order transition line. This nonentangled highly viscous and far from equilibrium liquidlike structure contrasts with the quasi-long-range positionally ordered vortex structures observed in pristine samples of the same compound at $T < T_{FOT}$ [39]. Experiments with significantly larger cooling times would allow us to ascertain whether a more ordered vortex structure is stable for a very dense distribution of CD.

Figure 6 shows a schematic picture for the relaxation dynamics of the defect-vortex forces. Within our model, the dynamics at T_{freez} is mainly controlled by DK excitations since most of the defect-vortex forces satisfy $f_s < f < f_d$, with $f_s \sim \gamma/d$ the force below which superkink excitations dominates. The parameter γ is the dispersion in pinning energies coming from the differences between columnar defects and from the disorder in their spatial distribution. In our model we have assumed that γ is negligible compared to U_0, so f_s is very small and superkink dynamics would become relevant only at very large time scales. If γ is not small, then the nonsteady relaxation may be dominated by variable range hops with DK becoming inefficient to irreversibly drive the vortices to a lower-energy state.

A previous work [38] proposes that the low-field vortex state nucleated in the case of a sample with a dense distribution of CD would not differ fundamentally from that observed in pristine samples. This is based in the finding that the energy difference between two metastable states in the former case is dominated by the vortex-vortex interaction energy rather than by the differences in pinning energy. Within this view, each vortex line is, however, confined and pinned to a CD. This proposal is similar to the one stating that the conventional Bose glass phase may have a crossover to a putative Bragg-Bose glass phase [42]. The later is a glassy phase with quasi-long-range order but confined in CD, and thus individual vortex lines are macroscopically flat, in sharp contrast to the rough vortex lines of the Bragg-glass phase expected for weak point disorder. Interestingly, our analysis suggests that the

truly glassy relaxation dynamics in our samples, such as the superkink or variable range hopping dynamics, or collective creep dynamics made of correlated hops (corresponding to one of the possible equilibrium phases), would become dominant only in the limit of very long relaxation times, much larger than the one probed during the magnetic decoration quenching process. These experiments, as they are currently done, can not give any information about the subjacent equilibrium phase expected at very long times. This will critically depend on the degree of dispersion of the pinning energies, $\gamma \sim f_s d$ [1].

Therefore, it would be interesting to implement glass-annealing techniques in order to reach configurations with a narrower distribution of vortex-defect forces and thus with less memory of the liquid phase and less accumulated stress. Observing the changes in the translational order of the decorated lattice as a function of the quenching time, for instance, may tell us which phase is more plausible, as the corresponding equilibrium correlation length slowly grows with time. In particular, if a topologically ordered equilibrium phase exists at low fields in the presence of a high density of CD or a discrete superconductor picture is valid, then the density of dislocations in the vortex structure should display a decrease with time. This effect might be seen, for instance, by comparing the number of ρ_{def} detected in magnetic decoration experiments performed at significantly different cooling rates.

VI. CONCLUSIONS

We have analyzed, through magnetic decoration images, dynamically frozen vortex configurations in heavy-ion irradiated $Bi_2Sr_2CaCu_2O_8$ samples with a very dense distribution of columnar defects. For low vortex densities compared with the CD density, we find an amorphous phase with liquidlike correlations, and an approximately Gaussian defect-vortex force distribution indicating a randomly oriented pinning scenario. By assuming vortices individually trapped at identical CD, we show that the observed translational order is fairly consistent with a relaxation dynamics dominated by DK excitations near the freezing temperature T_{freez}. Using a simple model and input from the $\mathbf{f}_i^{\mathrm{max}}$ experimental data obtained from magnetic decoration images, we predict a freezing temperature of the same order but smaller than the irreversibility temperature. We argue that magnetically decorated structures hence correspond to a typical configuration of a nonentangled vortex-liquid state with strongly reduced mobility, rather than to a metastable state of an equilibrium glassy phase with divergent relaxation barriers associated to the localization of vortices in CD even at very long times. Experiments with significantly larger cooling times or glass-annealing techniques are mandatory in order to deduce if, as expected, the equilibrium vortex phase nucleated in a very dense distribution of strong pins is a more ordered one.

ACKNOWLEDGMENTS

This work was made possible thanks to the support of the ECOS-Sud-MinCyT France-Argentina bilateral program, Grant No. A09E03. Work done at Bariloche was partially founded by PICT-PRH 2008-294 and University of Cuyo Reserch Grant No. 06-C381. A.B.K, D.D., and Y.F. also acknowledge support from ANPCyT-PICT-2011-1537.

[1] G. Blatter, M. V. Feigel'man, V. B. Geshkenbein, A. I. Larkin, and V. M. Vinokur, Rev. Mod. Phys. **66**, 1125 (1994).
[2] Y. Fasano, M. De Seta, M. Menghini, H. Pastoriza, and F. de la Cruz, Proc. Nat. Acad. Sci. USA **102**, 3898 (2005).
[3] A. P. Petrović, Y. Fasano, R. Lortz, C. Senatore, A. Demuer, A. B. Antunes, A. Paré, D. Salloum, P. Gougeon, M. Potel, and Ø. Fischer, Phys. Rev. Lett. **103**, 257001 (2009).
[4] Y. Fasano, J. Herbsommer, and F. de la Cruz, Phys. Stat. Sol. (b) **215**, 563 (1999).
[5] Y. Fasano, M. De Seta, M. Menghini, H. Pastoriza, and F. De la Cruz, Solid State Comm. **128**, 51 (2003).
[6] S. Demirdis, C. J. van der Beek, Y. Fasano, N. R. Cejas Bolecek, H. Pastoriza, D. Colson, and F. Rullier-Albenque, Phys. Rev. B **84**, 094517 (2011).
[7] C. J. van Der Beek, S. Demirdis, M. Konczykowski, Y. Fasano, N. R. Cejas Bolecek, H. Pastoriza, D. Colson, and F. Rullier-Albenque, Phys. B: Cond. Mat. **407**, 1746 (2012).
[8] S. Demirdis, Y. Fasano, S. Kasahara, T. Terashima, T. Shibauchi, Y. Matsuda, M. Konczykowski, H. Pastoriza, and C. J. van der Beek, Phys. Rev. B **87**, 094506 (2013).
[9] H. Yang, B. Shen, Z. Wang, L. Shan, C. Ren, and H.-H. Wen, Phys. Rev. B **85**, 014524 (2012).
[10] C. J. van Der Beek, S. Demirdis, D. Colson, F. Rullier-Albenque, Y. Fasano, T. Shibauchi, Y. Matsuda, S. Kasahara, P. Gierlowski, and M. Konczykowski, J. Phys. Conf. Series **449**, 012023 (2013).
[11] L. Civale, A. D. Marwick, M. W. McElfresh, T. K. Worthington, A. P. Malozemoff, F. H. Holtzberg, J. R. Thompson, and M. A. Kirk, Phys. Rev. Lett. **65**, 1164 (1990).
[12] M. Konczykowski, F. Rullier-Albenque, E. R. Yacoby, A. Shaulov, Y. Yeshurun, and P. Lejay, Phys. Rev. B **44**, 7167 (1991).
[13] C. J. van der Beek, *Thermodynamique des vortex dans les supraconducteurs desordonnes* (Südwestdeutscher Verlag für Hochschulschriften, Sarrebruck, 2010).
[14] D. R. Nelson and V. M. Vinokur, Phys. Rev. B **48**, 13060 (1993).
[15] C. J. van der Beek, M. Konczykowski, V. M. Vinokur, T. W. Li, P. H. Kes, and G. W. Crabtree, Phys. Rev. Lett. **74**, 1214 (1995).
[16] C. J. van der Beek, M. Konczykowski, V. M. Vinokur, G. W. Crabtree, T. W. Li, and P. H. Kes, Phys. Rev. B **51**, 15492 (1995); M. Konczykowski, N. Chikumoto, V. M. Vinokur, and M. V. Feigelman, *ibid.* **51**, 3957 (1995).
[17] J. C. Soret, V. T. Phuoc, L. Ammor, A. Ruyter, R. De Sousa, E. Olive, G. Villard, A. Wahl, and Ch. Simon, Phys. Rev. B **61**, 9800 (2000).
[18] M. Leghissa, L. A. Gurevich, M. Kraus, G. Saemann-Ischenko, and L. Ya. Vinnikov, Phys. Rev. B **48**, 1341 (1993).
[19] H. Dai, S. Yoon, J. Liu, R. C. Budhani, and Ch. M. Lieber, Science **265**, 1552 (1994).
[20] M. Menghini, Yanina Fasano, F. de la Cruz, S. S. Banerjee, Y. Myasoedov, E. Zeldov, C. J. van der Beek, M. Konczykowski, and T. Tamegai, Phys. Rev. Lett. **90**, 147001 (2003).

[21] S. S. Banerjee, A. Soibel, Y. Myasoedov, M. Rappaport, E. Zeldov, M. Menghini, Yanina Fasano, F. de la Cruz, C. J. van der Beek, M. Konczykowski, and T. Tamegai, Phys. Rev. Lett. **90**, 087004 (2003).

[22] M. Menghini, Yanina Fasano, F. de la Cruz, S. S. Banerjee, Y. Myasoedov, E. Zeldov, C. J. van der Beek, M. Konczykowski, and T. Tamegai, J. Low Temp. Phys. **135**, 139 (2004).

[23] S. S. Banerjee, A. Soibel, Y. Myasoedov, M. Rappaport, E. Zeldov, M. Menghini, Yanina Fasano, F. de la Cruz, C. J. van der Beek, M. Konczykowski, and T. Tamegai, Phys. C **408-410**, 495 (2004).

[24] Yanina Fasano, M. De Seta, M. Menghini, H. Pastoriza, and F. de la Cruz, Phys. C **408-410**, 520 (2004).

[25] M. Menghini, Yanina Fasano, F. de la Cruz, S. S. Banerjee, Y. Myasoedov, E. Zeldov, C. J. van der Beek, M. Konczykowski, and T. Tamegai, in *Perspectives on Superconductivity Research*, edited by P. S. Lewis (Nova Publishers, New York, 2005).

[26] F. Pardo, A. P. Mackenzie, F. de la Cruz, and J. Guimpel, Phys. Rev. B **55**, 14610 (1997).

[27] T. W. Li *et al.*, J. Cryst. Growth **135**, 481 (1994).

[28] A. Dorosinskii, M. V. Indenbom, V. I. Nikitenko, Yu A. Ossip'yan, A. A. Polyanskii, and V. K. Vlasko-Vlasov, Physica C **203**, 149 (1992).

[29] M. Konczykowski, F. Holtzberg, and P. Lejay, Supercond. Sci. Technol. **4**, S331 (1991).

[30] Y. Fasano and M. Menghini, Supercond. Sci. and Tech. **21**, 023001 (2008).

[31] H. Pastoriza, M. F. Goffman, A. Arribere, and F. de la Cruz, Phys. Rev. Lett. **72**, 2951 (1994).

[32] E. Zeldov, D. Majer, M. Konczykowski, V. B. Geshkenbein, V. M. Vinokur, and H. Shtrikman, Nature (London) **375**, 373 (1995).

[33] M. Konczykowski, C. J. van der Beek, A. E. Koshelev, V. Mosser, M. Dodgson, and P. H. Kes, Phys. Rev. Lett. **97**, 237005 (2006).

[34] J. Gilchrist and M. Konczykowski, Phys. C **212**, 43 (1993).

[35] N. Morozov, E. Zeldov, D. Majer, and M. Konczykowski, Phys. Rev. B **54**, R3784 (1996).

[36] M. I. Dolz, Y. Fasano, H. Pastoriza, V. Mosser, M. Li, and M. Konczykowski, Phys. Rev. B **90**, 144507 (2014).

[37] C. J. van der Beek, M. Konczykowski, R. J. Drost, P. H. Kes, N. Chikumoto, and S. Bouffard, Phys. Rev. B **61**, 4259 (2000).

[38] C. J. van der Beek, M. Konczykowski, A. V. Samoilov, N. Chikumoto, S. Bouffard, and M. V. Feigel'man, Phys. Rev. Lett. **86**, 5136 (2001).

[39] N. R. Cejas Bolecek, M. I. Dolz, A. Kolton, H. Pastoriza, C. J. van der Beek, M. Konczykowski, M. Menghini, G. Nieva, and Y. Fasano, J. Low Temp. Phys. **179**, 35 (2015).

[40] W. S. Seow, R. A. Doyle, A. M. Campbell, G. Balakrishnan, D. McK. Paul, K. Kadowaki, and G. Wirth, Phys. Rev. B **53**, 14611 (1996).

[41] A. Silhanek, L. Civale, S. Candia, G. Nieva, G. Pasquini, and H. Lanza, Phys. Rev. B **59**, 13620 (1999).

[42] T. Giamarchi and P. Le Doussal, Phys. Rev. B **55**, 6577 (1997).